Novel nanostructured Fe–Cu–Al trimetal oxide for enhanced antimony(V) removal: synthesis, characterization and performance

Jianyan Wang, Jing Chen, Qiumei Li and Gaosheng Zhang

ABSTRACT

Given the adverse health effects of antimony (Sb), there is an increased focus on developing methods to remove this toxic metal from contaminated water bodies. To effectively remove Sb(V), a new nanostructured Fe–Cu–Al trimetal oxide was fabricated using co-precipitation method at ambient temperature. The Fe–Cu–Al trimetal oxide was very effective at removing Sb(V) from water; it had a maximal adsorption capacity of 169.1 mg/g at pH 7.0, a capacity that was competitive with most other reported adsorbents. The obtained amorphous oxide had a high pH point of zero charge ($pH_{pzc} = 8.8$) and good adsorption Sb(V) efficiency over a wide pH range (4.0–8.0). Sb(V) uptake was achieved mainly through an ion-exchange reaction between Sb(V) ions and hydroxyl groups on the surface of the oxide. Given its good removal performance, high selectivity, and simple synthesis, this novel Fe–Cu–Al trimetal oxide offers a promising alternate for removing antimony contamination from aquatic environments.

Key words | adsorption, antimony(V), Fe–Cu–Al trimetal oxide, mechanism

Jianyan Wang
Jing Chen (corresponding author)
Key Laboratory of Coastal Environmental Processes and Ecological Remediation,
Yantai Institute of Coastal Zone Research (YIC),
Chinese Academy of Science (CAS),
Yantai 264003,
China
E-mail: *jchen@yic.ac.cn*

Jianyan Wang
University of Chinese Academy of Sciences,
19th A Yuquan Road, Beijing 100049,
China

Qiumei Li
School of Ocean,
Yantai University,
32th Qingquan Road, Yantai 264005,
China

Gaosheng Zhang
Key Laboratory of Water Safety and Protection in Pearl River Delta, Ministry of Education,
Guangzhou University,
Guangzhou 510006,
China

INTRODUCTION

Increased antimony (Sb) contamination in aquatic environments has heightened awareness of this potentially toxic metal. The natural occurrence of Sb, stemming from rock weathering and soil runoff, has been surpassed by contributions from anthropic activities including mining, smelting, the combustion of waste and fossil fuels, and waste disposal (Sun *et al.* 2016). In unpolluted fresh water, typical concentrations of dissolved antimony are less than 1 μg/L. In comparison, Sb in surface water collected near the Xikuangshan (China) antimony mine reached upward of 163 μg/L (Wang *et al.* 2011). Prolonged exposure to Sb compounds has a negative impact on human health, including myalgia, abdominal colic, skin rashes, dyspnea, and cardiotoxicity (Luo *et al.* 2015). Given the associated health risks, the permissible limits of antimonide as recommended by the US Environmental Protection Agency (USEPA) and the Chinese Ministry of Health are 6 μg/L and 5 μg/L, respectively. Thus, effective methods for removing Sb from contaminated water environments must be developed.

Antimony exists mainly in two oxidation states, Sb(III) and Sb(V), in aquatic environments. Both the mobility and solubility of Sb(V) are greater than that of Sb(III) as antimonate species exist mainly as $Sb(OH)_6^-$; thus, Sb(V) is harder to remove from aquatic settings (Li *et al.* 2018). Multiple methods have been suggested for purifying Sb(V)-contaminated water. These include coagulation-precipitation, electrochemical, membrane separation and adsorption approaches (Ungureanu *et al.* 2015; Ma *et al.* 2017). The adsorption method is superior to the other approaches due to its relatively low cost, high efficiency, and simple operation. Effective adsorbents have been developed for antimony removal, such as mineral adsorbents – goethite, kaolinite, gibbsite (Essington & Stewart 2015), and bentonite (Xi *et al.* 2011) – and single metal oxides, which includes hydrated ferric oxides (Miao *et al.* 2014), manganese oxide (Wang *et al.* 2018), and titanium dioxide (Yan *et al.* 2017). However, low adsorption capacities of these adsorbents

doi: 10.2166/wst.2019.198

and the long equilibrium time limit their application in Sb contaminated water treatments.

Considerable attention has been paid recently to composite metal adsorbents that contain two or more metal oxides. Mixed oxides are more active than single oxides for Sb(V) removal due to the synergistic effect between the metals. Iron oxides are well known as promising sorbent materials because of its high selectivity to Sb(V) and easy availability. Many iron-based composite oxides are being developed to remove Sb(V) from water. For example, Li *et al.* (2012) prepared a Fe–Zr bimetal oxide that exhibited a high antimonate adsorption capacity under acidic conditions. Xu *et al.* (2012) reported a Fe–Mn binary oxide having an Sb(V) adsorption capacity of 127.9 mg/g at pH 5.0, and Lu *et al.* (2015) produced a Zn–Fe double-layered hydroxide adsorbent having a maximum adsorption capacity of 122.03 mg/g for Sb(V) in a single-pollutant system. However, the high economic cost and narrow applicable range of pH limit their application in real water treatment processes.

Aluminum oxide is usually considered as having a high pH_{pzc}, as high as >8.0 (Valdivieso *et al.* 2006). When the surface of an oxide is positively charged, the adsorption of anions from the aqueous solution would be enhanced between the oxide and anions due to electrostatic attraction. Activated alumina has a good adsorption capacity for Sb(V) due to its marked binding affinity for Sb across a wide pH range (Xu *et al.* 2001). Dou *et al.* (2015) fabricated hierarchical macro/mesoporous amorphous alumina with an Sb(V) adsorption capacity of 118 mg/g. Moreover, cupric oxide also has a high pH_{pzc} and is an effective adsorbent for removing arsenic over a pH range of 6.5–8.5 (Zhang *et al.* 2013). Qi *et al.* (2016) synthesized a Cu-doped Fe_3O_4 adsorbent via a hydrothermal approach, and the incorporation of cupric oxide into the adsorbent increases Sb adsorption capacity from 7.07 mg/g of Fe_3O_4 to 30.92 mg/g. All told, there is much potential for combining aluminum and copper oxides with iron oxides to improve Sb(V) adsorption capacity at a relatively wide pH range.

Here, a new Fe–Cu–Al trimetal oxide containing iron oxide, cupric oxide and aluminum oxide was synthesized via a facile co-precipitation method to remove the Sb(V) from aqueous solution. Structural characteristics of this trimetal oxide were evaluated using a variety of techniques. Sb(V) adsorption behaviors were investigated by varying parameters such as Fe:Cu:Al molar ratio, initial Sb(V) concentration, contact time, solution pH, and coexisting ions. Moreover, a possible mechanism of Sb(V) removal by the developed Fe–Cu–Al trimetal oxide was elucidated.

METHODS AND MATERIALS

Materials

All chemicals used within the study were of analytical grade without further purification. The Sb(V) stock solution by dissolving appropriate amounts of potassium pyroantimonate ($KSbO_6H_6$) in deionized water. Solutions containing Sb were then adjusted to the required concentration by diluting samples of the prepared Sb(V) stock solution with deionized water.

Synthesis of the Fe–Cu–Al trimetal oxide

A series of Fe-Cu-Al trimetal oxide were synthesized at 4:1:1, 3:1:1, 2:1:1, 1:1:1, 1:1:2, 1:1:4, 1:1:6, 1:1:8 and 2:1:4 Fe:Cu:Al molar ratios at room temperature. The Fe-Cu-Al trimetal oxide adsorbent was prepared by a one-step simultaneous oxidation and coprecipitation method. Briefly, the main preparation procedure was as follows: predetermined amounts of $FeCl_3{\cdot}6H_2O$, $CuSO_4{\cdot}5H_2O$, and $Al_2(SO_4)_3{\cdot}18H_2O$ were dissolved in 400 mL of deionized water. Under vigorous magnetic-stirring, NaOH solution (2 mol/L) was added dropwise to raise the solution pH to a weak base. The formed suspension was stirred continuously for 30–60 min. After sitting at room temperature for 4 h, the suspension was washed several times with deionized water and then filtrated and dried at 55 °C for 24 h. The dried material was then crushed and stored as a fine powder in a desiccator.

Characterization of the Fe–Cu–Al trimetal oxide

The morphology of the Fe–Cu–Al trimetal oxide was characterized using an ultra-high-resolution field emission electron microscope (SEM, Merlin Compact, Germany) and a high-resolution transmission electron microscope (TEM, JEOL JEM-2100, Japan). X-ray diffraction (XRD) analysis was run on a D/Max-3A diffractometer (Rigaku Co., Japan) using Ni-filtered copper Kα radiation at 40 kV and 200 mA for the crystalline phase identification. The specific surface area of the Fe–Cu–Al trimetal oxide was determined via a nitrogen adsorption–desorption isotherm using the Brunauer–Emmett–Teller (BET) method with a Micromeritics ASAP 2020 surface area analyzer (Norcross, USA).

The Fourier transform infrared (FTIR) spectra of the Fe–Cu–Al trimetal oxide before and after reaction with the Sb(V) solution were collected using a Nicolet IS10 FTIR spectrophotometer (Thermo Scientific, USA) and a

transmission model. Samples used for FTIR determination were ground with spectral grade KBr in an agate mortar. All FTIR measurements were carried out at room temperature.

A zeta-potential analyzer (Zetasizer Nano-ZS90) was used to analyze the zeta potential of the Fe–Cu–Al trimetal oxide particles before and after Sb(V) adsorption. The content of Fe–Cu–Al trimetal oxide in the solution was 200 mg/L, and the Sb(V) concentration was 50 mg/L. The background electrolyte was 0.01 mol/L $NaNO_3$ to maintain a constant ionic strength. After 48 h of reaction to ensure that adsorption equilibrium was attained, the zeta potential of the suspension was measured via electrokinetic analysis.

The chemical states of the elements in the Fe–Cu–Al trimetal oxide before and after Sb treatment were assessed using X-ray photoelectron spectroscopy (XPS) with a monochromatized Al Kα as an exciting X-ray source (1,486.6 eV). XPS results were collected in binding energy forms and fitted using a nonlinear least squares curve-fitting program (XPSPEAK41 Software).

Batch adsorption experiments

To better evaluate the adsorption effect of Sb(V) on Fe–Cu–Al trimetal oxide, a series of adsorption experiments were conducted that included tests of adsorption-isotherms, adsorption kinetics, the effects of pH, ionic strength, and coexisting ions. All experiments, except for the kinetic experiment, were performed in 100 mL plastic vessels containing 50 mL of Sb(V) solution. During the experiment, the pH of the solution was adjusted using 0.1 mol/L of NaOH and HNO_3, and the vessels were shaken on an orbit shaker (170 rpm) at 25 ± 1 °C.

To determine the optimal Fe:Cu:Al molar ratio, batch tests were carried out to compare the adsorption capacity of Fe–Cu–Al trimetal oxides at different Fe:Cu:Al molar ratio. In each test, 10.0 mg of adsorbent sample was loaded into the 100 mL polyethylene bottles, containing 50 mL of 19.7 mg/L Sb(V) solution. The pH of the solutions was adjusted with 0.1 M NaOH or/and HNO_3 to around pH 7.0 ± 0.1 during the shaking process. Afterwards, the solutions were mixed on an orbit shaker at 170 rpm for 24 h.

The adsorption-isotherm experiments for Sb(V) were conducted at pH 7.0 ± 0.1 by adding the adsorbent at a dose of 200 mg/L. Initial Sb(V) concentrations varied from 5 mg/L to 60 mg/L. The background electrolyte of the solution was adjusted using 0.01 mol/L $NaNO_3$.

Adsorption kinetics were assessed using a background electrolyte of 0.01 mol/L $NaNO_3$ at a pH of 7.0 ± 0.1. To prepare a series of Sb(V) solutions having differing initial concentrations (5.1 mg/L, 10.5 mg/L, and 19.8 mg/L), defined amounts of Sb(V) stock solution and $NaNO_3$ were added to a 2,000 mL glass vessel and then diluted to 1,000 mL with deionized water. The Fe–Cu–Al trimetal oxides were added to attain a 200 mg/L solution that was mixed using a stirrer at an agitation speed of 170 rpm. Five-millimeter samples were collected from the solution at predetermined times and were filtered immediately through 0.45 μm membranes for analysis.

To investigate the influence of pH and ionic strength on Sb(V) adsorption, batch experiments were performed across a range of pH values (4.0–11.0) and with 0.001, 0.01, or 0.1 mol/L $NaNO_3$ as a background electrolyte concentration. The pH of the solution was adjusted every 2 h, and the equilibrium pH was measured. The effects of coexisting ions chloride, sulfate, bicarbonate, silicate, phosphate, calcium and magnesium on Sb(V) removal were investigated using an initial Sb(V) concentration of 9.1 mg/L at pH 7.0 ± 0.1. The concentration of coexisting ions ranged from 0.1–10 mmol/L.

All samples were filtered through 0.45 μm membrane filters after adsorption. The residual Sb(V) concentration of filtrate was analysed using an inductively coupled plasma mass spectrometry machine (ICP-MS, Elan DRC II, Perkin Elmer Co., USA). The samples were prepared for analysis by dissolution in a mixture of 2% nitric acid (HNO_3, sub-boiling distilled). Isotope Sb^{121} was selected as analyte and Y^{89} served as inner standard. All samples used in the analysis were analyzed within 24 h of collection.

RESULTS AND DISCUSSION

Characterization of the Fe–Cu–Al trimetal oxide

The SEM images (Figure 1(a) and 1(b)) show that Fe–Cu–Al trimetal oxide consists of multiple aggregated nanograins, which produce a rough surface. High-resolution TEM images (Figure 1(c) and 1(d)) demonstrate that these nanograins are formed from smaller nanosized particles that range from 50 to 200 nm and that have irregular shapes and amorphous structure. The EDS analysis (Figure S1, available with the online version of this paper) reveals that Fe, Cu and Al are evenly distributed on the surface and the molar ratio Fe:Cu:Al on the surface is about 1.09:1.00:3.96, which is very close to the value of 1:1:4 of the bulk Fe:Cu:Al molar ratio.

The N_2 adsorption–desorption isotherms (Figure S2, available online) of the Fe–Cu–Al trimetal oxide can be

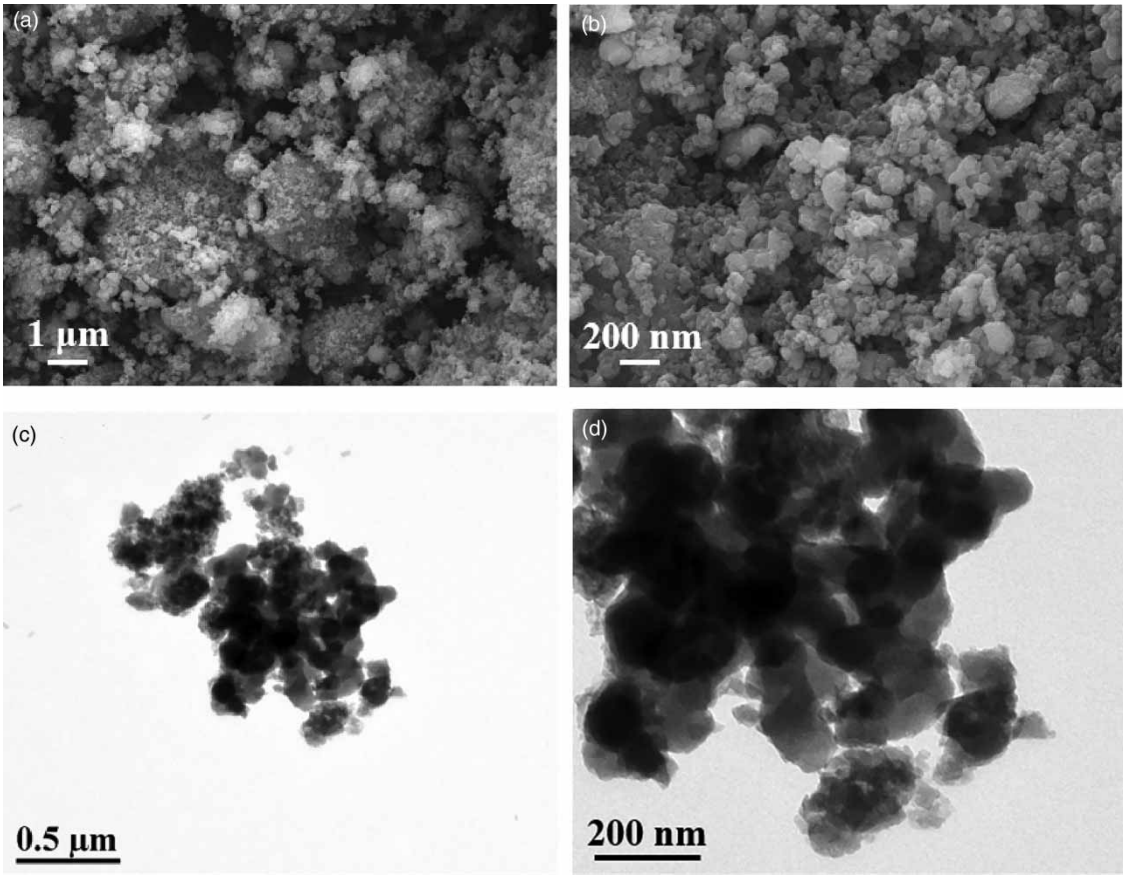

Figure 1 | Study of surfaces of the Fe–Cu–Al trimetal oxide: SEM image (a), (b); TEM image (c), (d).

assigned to type IV isotherms following IUPAC classification with a type H3 hysteresis loop; thus, these particles have a typical mesoporous structure (Xiang *et al.* 2016). The BET specific surface area of the synthesized Fe–Cu–Al trimetal oxide is 25.4 m^2/g. From the pore size distributions, the average pore diameter of Fe–Cu–Al trimetal oxide is 24.28 nm with a cumulative pore volume of 0.154 cm^3/g, determined by the Barrett–Joyner–Halenda (BJH) adsorption method. The mesoporous structure of the Fe–Cu–Al trimetal oxide would make it a promising candidate for the adsorption of pollutants.

Batch adsorption experiments

Effect of Fe:Cu:Al molar ratio on Sb(V) adsorption

To examine the effect of Fe:Cu:Al molar ratio on Sb(V) adsorption, a series of Fe–Cu–Al trimetal oxide adsorbents with Fe:Cu:Al molar ratio of 4:1:1, 3:1:1, 2:1:1, 1:1:1, 1:1:2, 1:1:4, 1:1:6, 1:1:8 and 2:1:4 were fabricated and tested for Sb(V) adsorption. As shown in Figure S3 (available online), Sb(V) adsorption by the Fe–Cu–Al trimetal oxide reaches a maximum capacity of approximately 96.9 mg/g when the ratio is 1:1:4. Although the value is slightly higher than that of 1:1:1 and 1:1:2 Fe–Cu–Al trimetal oxide, the economic cost would be lower than that of the other two oxides because of the higher proportion of aluminum oxide. Considering comprehensive adsorption effectiveness and cost, the Fe–Cu–Al trimetal oxide with Fe:Cu:Al molar ratio of 1:1:4 was chosen as feasible sorbent and used in the following sections.

Adsorption isotherms

It is important to evaluate the adsorption isotherms not only for understanding the interaction between the adsorbate and the adsorbent but also for designing the adsorption system. The adsorption-isotherm data are studied by the commonly used theoretical, nonlinear Langmuir and Freundlich adsorption isotherm models. The Langmuir model assumes that adsorption is limited to a single molecular layer, and all surface sites are homogeneously distributed and share the

same affinity for adsorption. The Freundlich model, on the other hand, assumes that the adsorbent is covered by a multilayer solute and that adsorption occurs on an energetically heterogeneous surface. The equations for the Langmuir (Equation (1)) and Freundlich models (Equation (2)) are expressed respectively as:

$$q_e = \frac{q_{max} K_L C_e}{1 + K_L C_e} \quad (1)$$

$$q_e = K_F C_e^{\frac{1}{n}} \quad (2)$$

where q_e and q_{max} are the amount of equilibrium adsorption capacity and the maximum adsorption capacity (mg/g), respectively; K_L (L/mg) is the equilibrium adsorption constant related to the affinity of binding sites; C_e is the equilibrium Sb(V) solution concentration (mg/L); K_F is roughly an indicator of the adsorption capacity; and n is the heterogeneity factor that has a lower value for more heterogeneous surfaces.

The adsorption constants obtained from the isotherms (Figure 2) are listed in Table 1. Higher regression coefficients suggest that the Langmuir isotherm model ($R^2 = 0.97$) is more suitable for describing the adsorption behavior than the Freundlich model ($R^2 = 0.84$). The large values of

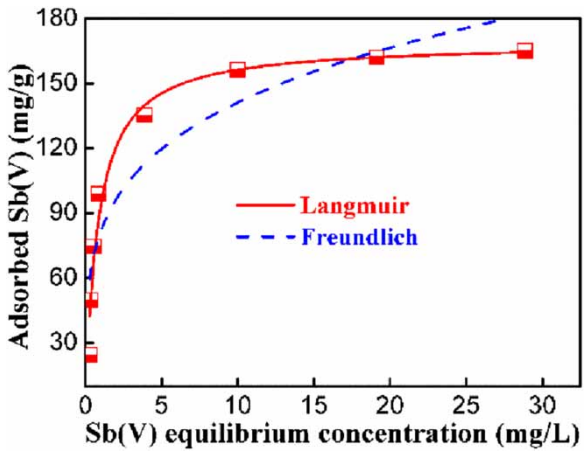

Figure 2 | Adsorption isotherms of Sb(V) by Fe–Cu–Al trimetal oxide. Adsorbent dose = 200 mg/L, pH = 7.0 ± 0.1, T = 25 ± 1 °C, equilibrium time = 24 h.

Table 1 | Langmuir and Freundlich isotherms parameters for Sb(V) adsorption on Fe–Cu–Al trimetal oxide

Langmuir model			Freundlich model		
q_{max} (mg/g)	K_L (L/mg)	R^2	K_F (L/g)	1/n	R^2
169.1	1.24	0.97	81.67	0.23	0.84

q_{max} and K_L demonstrate the high affinity of Sb(V) for the Fe–Cu–Al surface, implying a large number of available reactive sites for Sb(V) adsorption. The calculated maximal adsorption capacity for Sb(V) on the Fe–Cu–Al trimetal oxides is 169.1 mg/g at a pH of 7.0 ± 0.1. Compared to the adsorption capacities of other adsorbents reported in the literature (Table 2), the prepared Fe–Cu–Al trimetal oxide outperforms most other potential adsorbents. This heightens further the promise of Fe–Cu–Al trimetal oxides as effective adsorbent for removing Sb(V) from aqueous environments.

Adsorption kinetics

The kinetics of Sb(V) adsorption on the Fe–Cu–Al trimetal oxide has been investigated by batch experiments. The change of adsorbed Sb(V) as a function of contact time at three different initial concentrations is presented in Figure 3(a). The adsorption rate of Sb(V) happens during the first 4 hour and over 90% of the equilibrium adsorption capacity is achieved for the three different initial concentrations. This may be due to the freely available active-surface sites on the Fe–Cu–Al trimetal oxides and the higher concentration gradient of Sb(V) ions in the initial adsorption process. For the same adsorbent, a lower initial adsorbate concentration, at a constant adsorption rate, generally produces quicker adsorption, leading to a shorter time to equilibrium for the adsorption process. Furthermore, the residual Sb(V) was lower than the limit specified in the drinking water standard after 4 h, when Sb(V) initial concentration was 50 μg/L and adsorbent dose was 100 mg/L.

The pseudo-first-order model (Equation (3)) and the pseudo-second-order model (Equation (4)) simulate the kinetic data:

$$q_t = q_e(1 - e^{-k_1 t}) \quad (3)$$

$$q_t = \frac{q_e^2 k_2 t}{1 + q_e k_2 t} \quad (4)$$

where q_e and q_t are the adsorption capacities (mg/g) of the adsorbent at equilibrium and at any time t (h), respectively; k_1 (h^{-1}) and k_2 [g/(mg·h)] are the pseudo-first-order and pseudo-second-order rate constants for the adsorption process, respectively. From the related parameters of the two kinetic models (Table 3), the pseudo-second-order model explains accurately the kinetic data based on the correlation coefficients (R^2). This indicates that Sb(V) adsorption process might be chemisorption. Moreover, the high q_e coefficient and low k_2 constant also indicate strong Sb(V) adsorption on the Fe–Cu–Al trimetal oxides.

Table 2 | Maximum adsorption capacities (Q_{max}) reported in literature for antimony removal from aqueous solution

Adsorbents	Sb(V) con. range (mg/L)	Solution pH	Q_{max} for Sb(V) (mg/g)	Reference
Fe–Cu–Al trimetal oxide	0–60	7.0	169.1	Present study
Cu-doped Fe_3O_4	5–100	7.0	30.9	Qi *et al.* (2016)
Activated alumina	5–75	7.0	38	Xu *et al.* (2001)
ZrO_2–carbon nanofibers	10–500	7.0	57.2	Luo *et al.* (2015)
Fe–Zr binary oxide	0–25	7.0	60.4	Li *et al.* (2012)
Hydrated ferric oxides	5–70	6.0	62.5	Miao *et al.* (2014)
Mesoporous alumina	2–37	5.0	118	Dou *et al.* (2015)
Zn–Fe–LDH	2–100	7.0	122	Lu *et al.* (2015)
Fe–Mn binary oxide	12.2–121.8	5.0	127.9	Xu *et al.* (2012)
δ-MnO_2	0.12–24.36	7.0	140.8	Wang *et al.* (2018)
TiO_2	5–500	7.0	156	Yan *et al.* (2017)
Ce–doped Fe_3O_4	10–100	7.0	188.1	Qi *et al.* (2017)

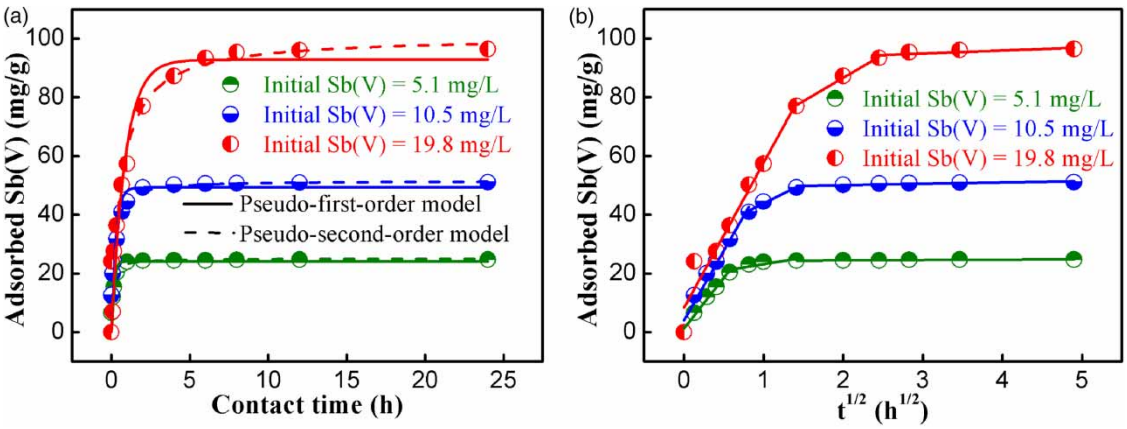

Figure 3 | Kinetics of Sb(V) adsorption on the Fe–Cu–Al trimetal oxide at pH = 7.0 ± 0.1: (a) fitted with the pseudo-first-order and pseudo-second-order models; (b) fitted with the intra-particle diffusion model. Adsorbent dose = 200 mg/L, equilibrium time = 24 h.

Table 3 | Kinetic parameters for Sb(V) adsorption on the Fe–Cu–Al trimetal oxide fitted with the pseudo-first-order and pseudo-second-order models

	Pseudo-first-order model			Pseudo-second-order model		
Initial Sb(V) concentration (mg/L)	q_e (mg/g)	k_1 (h^{-1})	R^2	q_e (mg/g)	k_2 (g/mg·h)	R^2
5.1	24.2	7.04	0.97	25.1	0.46	0.99
10.5	49.3	3.77	0.94	51.6	0.12	0.97
19.8	92.8	1.15	0.94	100.8	0.02	0.96

For a well-stirred system, intraparticle diffusion is always slow and is the rate-determining step. Thus, the intraparticle diffusion model (Equation (5)) was used to evaluate this limiting step based on the kinetic data.

$$q_t = k_p t^{\frac{1}{2}} + C \quad (5)$$

where q_t is the adsorption capacity at any time t (h), k_p is the intraparticle diffusion rate constant, and the constant C (mg/g) represents the boundary layer effect. Both k_p and C can be determined from the plot of q_t versus $t^{1/2}$.

The plot of Sb(V) adsorbed versus the square root of time (Figure 3(b)) shows a multilinear correlation, implying that three stages occur during the adsorption process: the boundary diffusion step, the intraparticle step (solute from the adsorbent surface to the intraparticle active sites), and the final equilibrium step. If intraparticle diffusion is the

rate-controlling step, the plot of q_t against $t^{1/2}$ should be linear and pass through the origin. However, as the value of C (see Table S1, available online) is much higher than 0 and increases proportionally with boundary layer thickness, it is deduced that Sb(V) adsorption is a multistep process, Both boundary and intraparticle diffusion are the adsorption rate-limiting steps.

Effects of solution pH and ionic strength

The pH of the solution influences the surface charge of both adsorbents and Sb(V) species. Assessing the effect of solution pH on Sb(V) removal by the Fe–Cu–Al trimetal oxide (Figure 4), it is observed that the adsorption capacity of Sb(V) depends on pH values; the greatest adsorption occurs under acidic conditions. The removal efficiency of Sb(V) is greater than 95% when pH ranges from 4.5–6.5. However, the removal capacity of Sb(V) decreases sharply as pH increases (9.5–10.5). These results are consistent with pH-dependent Sb(V) speciation and the surface charge of the Fe–Cu–Al trimetal oxide. In acid systems, Sb(V) aqueous speciation is controlled by hydrolysis (Wilson *et al.* 2010):

$$Sb(OH)_5^0 + H_2O = Sb(OH)_6^- + H^+ (\log Ka = -2.7) \quad (6)$$

Thus, the hydroxyl anion $Sb(OH)_6^-$ species predominate at pH values >2.7 (Ungureanu *et al.* 2015). Given the negatively charged Sb(V) species and positively charged Fe–Cu–Al trimetal oxide surface ($pH_{pzc} = 8.8$ in zeta potential measurements, Figure 5), Sb(V) adsorption capacity is facilitated by electrostatic attraction under acidic conditions. In contrast, the removal efficiency of Sb(V) decreases gradually

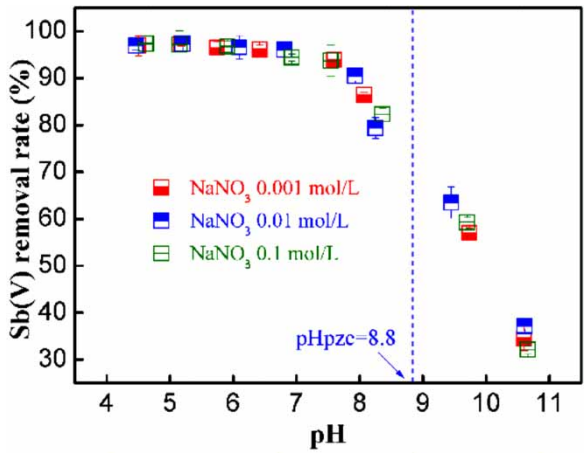

Figure 4 | Effects of pH and ionic strength on Sb(V) adsorption by Fe–Cu–Al trimetal oxide. Initial Sb(V) concentration = 9.1 mg/L, adsorbent dose = 200 mg/L, equilibrium time = 24 h.

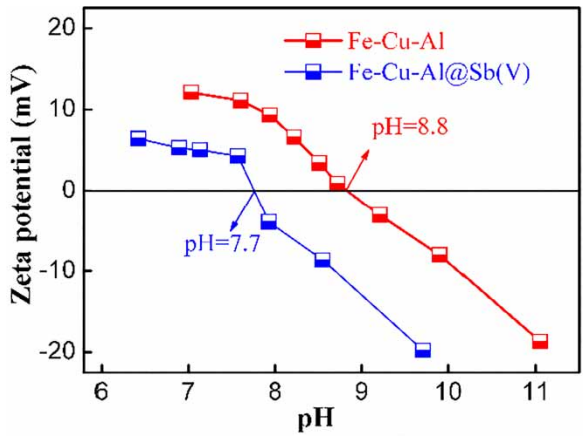

Figure 5 | Zeta potential of Fe–Cu–Al trimetal oxide before and after Sb(V) adsorption. Initial Sb(V) concentration = 50 mg/L; adsorbent dosage = 200 mg/L and equilibrium time = 48 h.

at pH >6.5 and especially at pH >9.0. This pattern may be related to the electrostatic repulsion between Sb(V) species [$Sb(OH)_6^-$] and negatively charged Fe–Cu–Al trimetal oxide surfaces at a solution pH above pH_{pzc}, and the fierce competition between Sb(V) species and hydroxyls at high pH values (Zhao *et al.* 2014).

No significant change is found for antimonate adsorption as the ionic strength increases from 0.001 to 0.1 mol/L (Figure 4). Ions adsorbed by outer-sphere associations through electrostatic forces are sensitive to variations in ionic strength. Ions adsorbed by inner-sphere associations show either little sensitivity to ionic strength or respond to higher ionic strengths with greater adsorption. From this pattern, it can be concluded that antimonate may be specifically adsorbed onto Fe–Cu–Al trimetal oxide via the forming of inner-sphere surface complexes.

Effect of coexisting ions

Adsorption selectivity is a key factor influencing removal effectiveness. Coexisting ions such as chloride, sulfate, bicarbonate, silicate, phosphate, calcium and magnesium are generally present in groundwater, and may influence Sb(V) adsorption by competing for adsorptive sites on the adsorbent surface. The effect of these coexisting ions on Sb(V) adsorption are shown in Figure S4 (available online). The presence of chloride has a negligible effect on adsorption capacity. For sulfate and bicarbonate, only a slight decrease is observed as their concentrations increase. However, both silicate and phosphate show a significant inhibitory effect on Sb(V) removal, especially at high concentrations. This could be due to the strong competition for the active adsorption

sites between silicate/phosphate ions and antimony species. However, calcium and magnesium enhance Sb(V) removal from aqueous solutions. It was believed that coexisting cations can be adsorbed on the surface of the adsorbent resulted in a positive charged surface, which favored the adsorption of anionic species (Zhang *et al.* 2009). More Sb(V) can be adsorbed on the surface of the adsorbent by enhancing the direct electrostatic force between the surface of the adsorbent and Sb(V) anions.

Adsorption mechanisms

Measurement of zeta potential

The zeta potential of Fe–Cu–Al trimetal oxide with and without adsorbed Sb(V) as a function of pH is shown in Figure 5. Fe–Cu–Al trimetal oxide has a relatively high pH_{pzc} of 8.8, possibly related to the incorporation of aluminum oxide. After adsorption of Sb(V), this value decreases to about 7.7. The specific adsorption of anions makes the surface of the oxide more negatively charged; this shifts the pH_{pzc} to a lower value. Thus, specific adsorption, rather than pure electrostatic interaction, is confirmed (Stumm & Morgan 1996).

Analysis of X-ray diffraction pattern

The X-ray diffraction pattern of Fe–Cu–Al trimetal oxide shows two peaks for the adsorbent at 10.4° and 20.8° (Figure S5, available online), typical for amorphous aluminum hydroxides (Wang *et al.* 2017). A weak peak at 35.6° indicates the combination of ferric and cupric hydroxide (Wang *et al.* 2015). Furthermore, there is a broad peak at 63.4° attributed to poorly ordered two-line ferrihydrite. This suggests that Fe–Cu–Al trimetal oxide is amorphous, which is consistent with the TEM data. After adsorption, one peak of aluminum hydroxides at 10.4° turns to a weak broad peak at 9.7°. Moreover, its another peak at 20.8° shifts to 19.5° and enhances. Simultaneously, the peaks of ferric and cupric hydroxide weaken slightly. These changes indicate an interaction of Sb(V) with these three metal oxides, especially with aluminum hydroxides.

Analysis of FTIR spectra

The FTIR spectra of the Fe–Cu–Al trimetal oxide before and after adsorption of Sb(V) are illustrated in Figure 6. It was found that the samples exhibit two bands located at 3,434 cm^{-1} and 1,650 cm^{-1}, which are ascribed to the vibration of H–O–H stretching and the bending vibration of water molecules, respectively. These bands indicate the presence of physisorbed water molecules on the adsorbents. However, the intensity and position of these peaks show almost no change after Sb(V) adsorption. This suggests that the influence of physically adsorbed water molecules is negligible on the uptake of Sb(V). Adsorption bands at 1,130 cm^{-1} and 971 cm^{-1} correspond to the bending vibration of the hydroxyl group associated with Fe (Ren *et al.* 2011). The peak at 603 cm^{-1} is associated with the stretching modes of Cu–OH. In addition, a clear characteristic peak at 544 cm^{-1} is assigned to the stretching vibration mode of Al–O (Lv *et al.* 2013). After reaction with Sb(V), peaks at 1,130 cm^{-1}, 603 cm^{-1}, and 544 cm^{-1} are all slightly weakened. These peaks indicate an interaction of the Sb(V) with the Fe–OH, Al–OH, and Cu–OH sites, respectively.

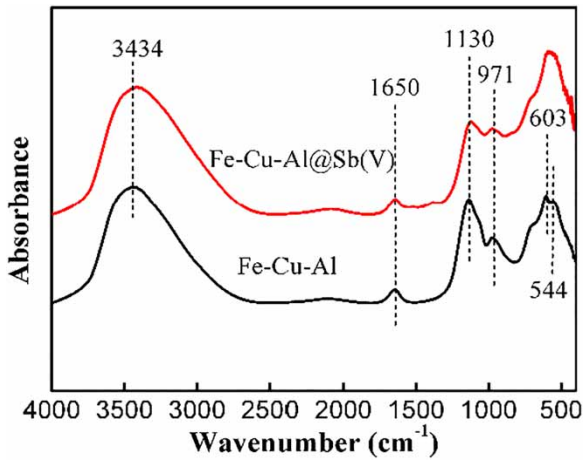

Figure 6 | FTIR diffraction pattern of Fe–Cu–Al trimetal oxide before and after Sb(V) adsorption.

XPS characterization

The XPS spectra for Fe 2p, Cu 2p, Al 2p, and Sb 3d are used to investigate the composition and chemical state of the Fe–Cu–Al trimetal oxide before and after reaction with Sb(V) (Figure S6, available online). For Fe 2p, the binding energy at 711 eV is attributed to the Fe(III) oxide (Glisenti 2000). The peaks of Cu 2p, located at 932.8 eV and 952.6 eV, are assigned to Cu $2p_{3/2}$ and Cu $2p_{1/2}$, respectively (Peng *et al.* 2016). The Al 2p binding energy at 74.3 eV corresponds to Al oxide, which has binding energy generally between 73.5 eV and 75.5 eV (Lv *et al.* 2013). After Sb(V) adsorption, the binding energy of Fe, Cu, and Al change minimally, indicating that no redox reaction occurs during the adsorption process. The

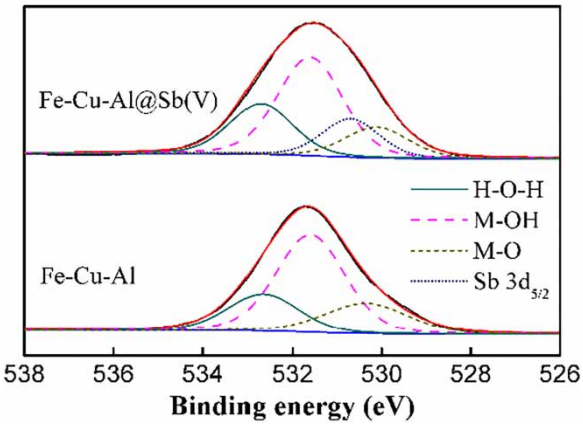

Figure 7 | O 1s XPS spectra of Fe–Cu–Al trimetal oxide before and after reaction with Sb(V).

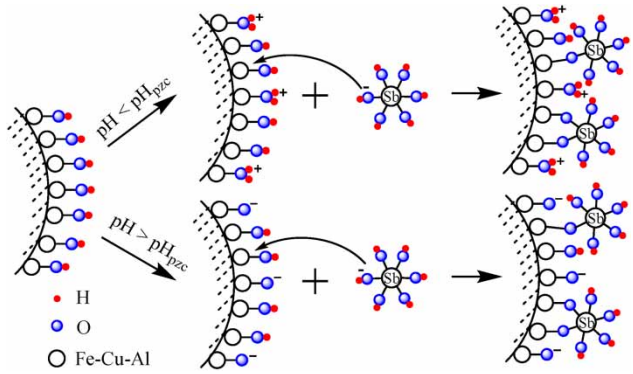

Figure 8 | Schematic diagram of Sb(V) adsorption on Fe–Cu–Al trimetal oxide.

Sb 3d spectra have peak binding energy at 530.7 and 539.8 eV corresponding to Sb $3d_{5/2}$ and Sb $3d_{3/2}$, respectively. This pattern indicates that Sb(V) has been chemically adsorbed onto the surface of the Fe–Cu–Al trimetal oxide (Luo *et al.* 2015).

The high-resolution scan of O 1s spectra can be decomposed into three peaks for lattice oxygen (M–O), hydroxyl (M–OH), and adsorbed water (H–O–H) (Figure 7). Hydroxyl is the most abundant (531.60 eV, 56.72%), followed by adsorbed water (532.65 eV, 21.86%), and then lattice oxygen (530.35 eV, 21.42%) in Fe–Cu–Al trimetal oxide. After adsorption, the percentage of H–O–H is almost unchanged, revealing again that the adsorbed water molecules have a negligible effect on the removal of Sb(V). However, the M–OH content is significantly changed, and the percentage of M–OH in Fe–Cu–Al trimetal oxide decreases from 56.72% to 46.84%. Therefore, the hydroxyl groups – a key contributor to Sb(V) adsorption by metal oxides – are replaced by antimonic species during the adsorption on Fe–Cu–Al trimetal oxide.

Based on the above mentioned analysis, a mechanism for Sb(V) adsorption on Fe–Cu–Al trimetal oxide was proposed as shown in Figure 8. The M–OH groups on the surface of Fe–Cu–Al trimetal oxide play a key role in Sb(V) uptake. The $Sb(OH)_6^-$ is transported to the solid/water interface from the bulk solution. Then, an ion-exchange reaction occurs between $Sb(OH)_6^-$ and the M–OH group to form the inner-surface complex.

CONCLUSION

A novel nanostructured Fe–Cu–Al trimetal oxide with an Fe:Cu:Al molar ratio of 1:1:4 is synthesized via a simple coprecipitation method. The maximal adsorption capacity of Sb(V) is 169.1 mg/g at pH 7.0, a higher value than other adsorbents. Optimal performance is obtained when the solution pH ranges 4.0–8.0 due to the high pH_{pzc} of the Fe–Cu–Al trimetal oxide. The adsorbent has a high selectivity in Sb(V) adsorption and coexisting ions – except for silicate and phosphate – do not affect Sb(V) uptake. Zeta potential measurements, FTIR, and XPS confirm that the abundant surface hydroxyl groups (M–OH) attribute to the high uptake of Sb(V) and the formation of inner-sphere surface complexes. Given its good Sb(V) removal, high selectivity, and simple synthesis process, the obtained Fe–Cu–Al trimetal oxide is a novel and promising adsorbent for removing Sb(V) from contaminated aquatic environments.

ACKNOWLEDGEMENTS

This work was financially supported by the National Natural Science Foundation of China (Grants No. 51478457 and 51678562).

REFERENCES

Dou, X., Mohan, D. & Zhao, X. 2015 Antimonate removal from water using hierarchical macro-/mesoporous amorphous alumina. *Chen. Eng. J.* **264**, 617–624.

Essington, M. E. & Stewart, M. A. 2015 Influence of temperature and pH on antimonate adsorption by gibbsite, goethite, and kaolinite. *Soil Sci.* **180**, 54–66.

Glisenti, A. 2000 The reactivity of a Fe–Ti–O mixed oxide under different atmospheres: study of the interaction with simple alcohol molecules. *J. Mol. Catal. A-Chem.* **153**, 169–190.

Li, X., Dou, X. & Li, J. 2012 Antimony(V) removal from water by iron-zirconium bimetal oxide: performance and mechanism. *J. Environ. Sci-China.* **24**, 1197–1203.

Li, J., Zheng, B., He, Y., Zhou, Y., Chen, X., Ruan, S., Yang, Y., Dai, C. & Tang, L. 2018 Antimony contamination, consequences and removal techniques: a review. *Ecotox. Environ. Safe.* **156**, 125.

Lu, H., Zhu, Z., Zhang, H., Zhu, J. & Qiu, Y. 2015 Simultaneous removal of arsenate and antimonate in simulated and practical water samples by adsorption onto Zn/Fe layered double hydroxide. *Chen. Eng. J.* **276**, 365–375.

Luo, J., Luo, X., Crittenden, J., Qu, J., Bai, Y., Peng, Y. & Li, J. 2015 Removal of antimonite (Sb(III)) and antimonate (Sb(V)) from aqueous solution using carbon nanofibers that are decorated with zirconium oxide (ZrO_2). *Environ. Sci. Technol.* **49**, 11115–11124.

Lv, J., Liu, H., Liu, R., Zhao, X., Sun, L. & Qu, J. 2013 Adsorptive removal of phosphate by a nanostructured Fe–Al–Mn trimetal oxide adsorbent. *Powder Technol.* **233**, 146–154.

Ma, B., Wang, X., Liu, R., Jefferson, W. A., Lan, H., Liu, H. & Qu, J. 2017 Synergistic process using Fe hydrolytic flocs and ultrafiltration membrane for enhanced antimony(V) removal. *J. Membrane Sci.* **537**, 93–100.

Miao, Y., Han, F., Pan, B., Niu, Y., Nie, G. & Lv, L. 2014 Antimony(V) removal from water by hydrated ferric oxides supported by calcite sand and polymeric anion exchanger. *J. Environ. Sci-China.* **26**, 307–314.

Peng, B., Song, T. T., Wang, T., Chai, L. Y., Yang, W. C., Li, X. R., Li, C. F. & Wang, H. Y. 2016 Facile synthesis of Fe_3O_4@$Cu(OH)_2$ composites and their arsenic adsorption application. *Chem. Eng. J.* **299**, 15–22.

Qi, Z., Lan, H., Joshi, T. P., Liu, R., Liu, H. & Qu, J. 2016 Enhanced oxidative and adsorptive capability towards antimony by copper-doping into magnetite magnetic particles. *RSC Adv.* **6**, 66990–67001.

Qi, Z., Joshi, T. P., Liu, R., Liu, H. & Qu, J. 2017 Synthesis of Ce(III)–doped Fe_3O_4, magnetic particles for efficient removal of antimony from aqueous solution. *J. Hazard. Mater.* **329**, 193–204.

Ren, Z., Zhang, G. & Chen, J. P. 2011 Adsorptive removal of arsenic from water by an iron-zirconium binary oxide adsorbent. *J. Colloid Interf. Sci.* **358**, 230–237.

Stumm, W. & Morgan, J. 1996 *Aquatic Chemistry: Chemical Equilibria and Rates in Natural Waters*. John Wiley & Sons, Inc., New York, NY, USA.

Sun, W., Xiao, E., Dong, Y., Tang, S., Krumins, V., Ning, Z., Sun, M. & Xiao, T. 2016 Profiling microbial community in a watershed heavily contaminated by an active antimony (Sb) mine in Southwest China. *Sci. Total Environ.* **550**, 297–308.

Ungureanu, G., Santos, S., Boaventura, R. & Botelho, C. 2015 Arsenic and antimony in water and wastewater: overview of removal techniques with special reference to latest advances in adsorption. *J. Environ. Manage.* **151**, 326–342.

Valdivieso, A. L., Bahena, J. L. R., Song, S. & Urbina, R. H. 2006 Temperature effect on the zeta potential and fluoride adsorption at the alpha–Al_2O_3/aqueous solution interface. *J. Colloid Interf. Sci.* **298**, 1–5.

Wang, X., He, M., Xi, J. & Lu, X. 2011 Antimony distribution and mobility in rivers around the world's largest antimony mine of Xikuangshan, Hunan Province. *China Microchem. J.* **97**, 4–11.

Wang, T., Yang, W., Song, T., Li, C., Zhang, L., Wang, H. & Chai, L. 2015 Cu doped Fe_3O_4 magnetic adsorbent for arsenic: synthesis, property, and sorption application. *RSC Adv.* **5**, 50011–50018.

Wang, M., Yu, X., Yang, C., Yang, X., Lin, M., Guan, L. & Ge, M. 2017 Removal of fluoride from aqueous solution by Mg–Al–Zr triple-metal composite. *Chem. Eng. J.* **322**, 246–253.

Wang, H., Wang, Y., Sun, Y., Pan, X., Zhang, D. & Tsang, Y. F. 2018 Differences in Sb(V) and As(V) adsorption onto a poorly crystalline phyllomanganate (δ-MnO_2): adsorption kinetics, isotherms, and mechanisms. *Process Saf. Environ.* **113**, 40–47.

Wilson, S., Lockwood, P., Ashley, P. & Tighe, M. 2010 The chemistry and behaviour of antimony in the soil environment with comparisons to arsenic: a critical review. *Environ. Pollut.* **158**, 1169–1181.

Xi, J., He, M. & Lin, C. 2011 Adsorption of antimony(III) and antimony(V) on bentonite: kinetics, thermodynamics and anion competition. *Microchem. J.* **97**, 85–91.

Xiang, B., Ling, D., Lou, H. & Gu, H. 2016 3D hierarchical flower-like nickel ferrite/manganese dioxide toward lead (II) removal from aqueous water. *J. Hazard. Mater.* **325**, 178–188.

Xu, Y., Ohki, A. & Maeda, S. 2001 Adsorption and removal of antimony from aqueous solution by an activated Alumina. *Toxicol. Environ. Chem.* **80**, 133–144.

Xu, W., Liu, R. & Qu, J. 2012 The adsorption behaviors of Fe–Mn binary oxide towards Sb(V). *Acta Scien. Circum.* **32**, 270–275.

Yan, L., Song, J., Chan, T. & Jing, C. 2017 Insights into antimony adsorption on {001}TiO_2: XAFS and DFT study. *Environ. Sci. Technol.* **51**, 6335–6341.

Zhang, G., Liu, H., Liu, R. & Qu, J. 2009 Adsorption behavior and mechanism of arsenate at Fe-Mn binary oxide/water interface. *J. Hazard. Mater.* **168**, 820–825.

Zhang, G., Ren, Z., Zhang, X. & Chen, J. 2013 Nanostructured iron(III)–copper(II) binary oxide: a novel adsorbent for enhanced arsenic removal from aqueous solutions. *Water Res.* **47**, 4022–4031.

Zhao, X., Dou, X., Mohan, D., Pittman, C., Ok, Y. & Jin, X. 2014 Antimonate and antimonite adsorption by a polyvinyl alcohol-stabilized granular adsorbent containing nanoscale zero-valent iron. *Chem. Eng. J.* **247**, 250–257.

First received 9 January 2019; accepted in revised form 3 June 2019. Available online 13 June 2019